Chapter 5

Wetting and Navier-Stokes Equation — The Manufacture of Composite Materials

Mario Caccia, Antonio Camarano, Danilo Sergi, Alberto Ortona and Javier Narciso

Additional information is available at the end of the chapter

http://dx.doi.org/10.5772/61167

Abstract

It is well known that there are several processes to manufacture composite materials, a large part of which consist in the infiltration of a liquid (matrix) through a porous medium (reinforcement). To perform these processes, both thermodynamics (wetting) and kinetics (Navier-Stokes) must be considered if a good quality composite material is sought. Although wetting and the laws that govern it have been well known for over 200 years, dating back to the original works of Young and Laplace, this is not the case with the Navier-Stokes equation, which remains so far unsolved. Although the Navier-Stokes equation, which describes the motion of a fluid, has been solved for many particular cases, such as the motion of a fluid through a pipe, which has resulted in the well-known Poiseuille equation, or the motion of a fluid through a porous media, described by the Darcy's law (empirical law obtained by Darcy), its general solution remains one of the greatest challenges of mathematicians today. Therefore, the objective of this chapter is to present the resolution of the Navier-Stokes equation with the laws of wetting for different cases of interest in the manufacture of composite materials.

Keywords: Wettability, Infiltration, Navier-Stokes

1. Introduction

Composite materials are an important and oftentimes used type of engineering materials with tuneable properties which depend on the materials combined. They are usually made of two

or more materials. The first phase, commonly referred to as "reinforcement" is constituted by a solid material, which can be employed in several morphologies such as fibers (short or continuous), particles, or as a co-continuous domain of a solid phase which occupies a fraction of the available volume (foams) [1-7]. The second phase, normally called "matrix," can be gaseous, liquid, or solid, and is in contact with the reinforcement through a proper interface. Composite materials are very common in nature, where a combination of fibers and matrix is often found. A good example is wood, which is composed of flexible fibers of cellulose embedded in a rigid matrix of lignin. Artificially produced composites are usually classified, according to the nature of their matrix, into metal, ceramic, or polymer matrix composites. Each type of composite presents its advantages and disadvantages, and together they cover a great scope of applications [1, 8-12].

Composite materials manufacturing can be accomplished through several techniques. Each technique is mainly the result of the trade-off between the target properties of the final product, the starting materials properties, and the final cost. In most of the cases, the matrix is in a liquid state during processing. A common action in composite materials manufacturing is "to infiltrate" the reinforcement with the matrix. When a liquid is used, the impregnation of the remaining free volume is highly dependent on how the first phase is placed in the space and on the physical properties of the liquid itself. In the case of polymeric matrix composites (PMC) techniques involving a liquid matrix are the only way to process them, as polymers are in a liquid state before their cross-linking in thermosets, or can be melted if they are thermoplastics. Also, ceramic matrix composites are processed through liquid routes (e.g., sol-gel techniques for oxide composites, or polymer infiltration and pyrolysis (PIP) [13-14] for ceramic matrix composites (CMC) produced by pre-ceramic precursors. In the latter case, where several impregnations are performed, the permeability of the porous materials decreases with the increasing of the final density of the composite under production). A widely utilized technique which stands among ceramic and metallic matrix composites (MMC) manufacturing is the so-called reactive silicon infiltration [15]. Its peculiarity is that, during processing, silicon is molten and by reacting with extra carbon present in the primary phase it yields silicon carbide. This method was not originally conceived to produce composite materials, but for the synthesis of bulk SiC, still, it proved to be a suitable methodology for ceramic matrix composites manufacture as well.

Some industrial products obtained with this infiltration technology are pantographs, connecting rods, loudspeakers, piston rings, heat sinks, electro-brushes, engine cylinders, brake discs, etc. In most of these examples, primary phase (reinforcement) content is above 50% in volume. For reinforcement contents of such magnitude, the most commonly used technique for manufacturing composites is infiltration [1, 5-7, 16-18].

Actually, infiltration processes are not exclusive of materials manufacture, but can be observed in many everyday life activities, such as making coffee, where hot water is infiltrated into a porous bed of coffee particles. Perhaps one of the most important cases where infiltration phenomenon is observed is in the penetration of rainwater into the ground, which ends up filling aquifers that guarantee water supply to population in dry regions where the surface runoff is scarce. Because of the great importance of infiltration in geological sciences, it was in

http://dx.doi.org/10.5772/61167

this field where the deepest and most detailed studies of this phenomenon were performed. Many advances in this area of knowledge have been expanded and applied to other scientific fields such as materials science. The clearest example is Darcy's law which is widely used in the design of composite materials. This empirical law was obtained by Henry Darcy whose original work published in 1856 is entitled: *"Les Fontaines Publiques de la Ville de Dijon"* (The Public Fountains of the City of Dijon). However, Darcy's law is not the only example that can be found in the literature. The relationship between water saturation and organic compounds in soils of different origins has resulted in the semiempirical equations of Brooks and Corey [19] and Van Genuchten [20], both widely used in composite materials.

The aim of the present chapter is to introduce the reader to the basic concepts of wetting and infiltration, and to combine these concepts to solve the equations governing the infiltration process in several particular cases that often arise in the composite materials manufacturing industry.

2. Experimental

Although it will be discussed in detail in the upcoming sections of the chapter, it is important to clarify that infiltration, in most composite materials manufacturing processes, does not occur spontaneously (in the case of PMCs it does proceed spontaneously, but it is so slow that it is necessary to force it), so the liquid must be forced to infiltrate by applying an external pressure. From an engineering point of view, mainly two technologies have been developed for this purpose: the so-called gas-assisted pressure infiltration (GPI), where a gas is used to push the liquid; and another called squeeze-casting (SC) in which pressure is applied by means of a mechanical device. Each technique has its upsides and downsides, which will be discussed throughout this chapter. The main advantage of GPI over SC is that it allows a better control of physical parameters (pressure and temperature), and admits higher complexity in the manufactured parts. On the other hand, the main advantage of SC over GPI is that higher pressures can be achieved and the automatization of the process becomes easier.

First the GPI technique will be analyzed, and for this purpose, the example of a laboratory equipment developed at the University of Alicante will be used [10, 11, 21-29]. A scheme of the equipment is shown in Figure 1. The equipment consists of a pressure chamber (maximum admissible pressure at 300 °C of 5 MPa) equipped with a resistance furnace, which is thermally isolated from the chamber by the use of conventional refractory material (temperature of chamber wall is always below 100°C). The furnace has a power of 1500 W and can reach temperatures of 1000°C. For measurement and control of furnace temperature, K type thermocouples, connected to a temperature controller, are used. The pressure control is entirely performed by a system of pneumatic and electronic valves connected to a pressure controller. The pressure vessel is made entirely of stainless steel and consists of a cylindrical body with an internal diameter of 30 cm, an outer diameter of 34.6 cm, a height of 45 cm, and a wall thickness of 3 cm. The closing of the camera is made with 12 M16 mounting studs. Both, the electrical feed (to thermocouple input and power cables) and the gas inlet and outlet for

pressurizing the chamber are positioned in the body. Additionally, the camera is connected to a primary vacuum pump, which allows the process to be performed in the absence of oxygen (low partial pressure).

The manufacturing process of a composite material using GPI can be described as follows: a preform, which consists of a porous bed of compacted particles, is placed into a quartz (or BN-coated graphite) crucible and a metal ingot is placed on top of it (see Figure 1b). The crucible is then introduced inside the pressure chamber and vacuum is applied during at least 30 min., until a pressure of about 100 Pa is reached. The chamber is heated under vacuum at a very low rate (3°C/min) up to 250°C, to remove humidity and gas adsorbed on particles. Subsequently, further heating is applied up to a temperature 50°C higher than the melting point of the metal at a rate of approximately 5°C/min. The maximum temperature is then maintained for 30 min followed by argon injection to reach the desired infiltration pressure. Once the preform has been infiltrated (approximately 2 min. under pressure) the crucible is pushed towards the bottom of the chamber, which is cold, and directional solidification occurs, ensuring a high-quality composite (null porosity). Figure 2 shows a composite material obtained at the University of Alicante with this process, where it is possible to observe the absence of porosity and an intimate contact between reinforcement and matrix.

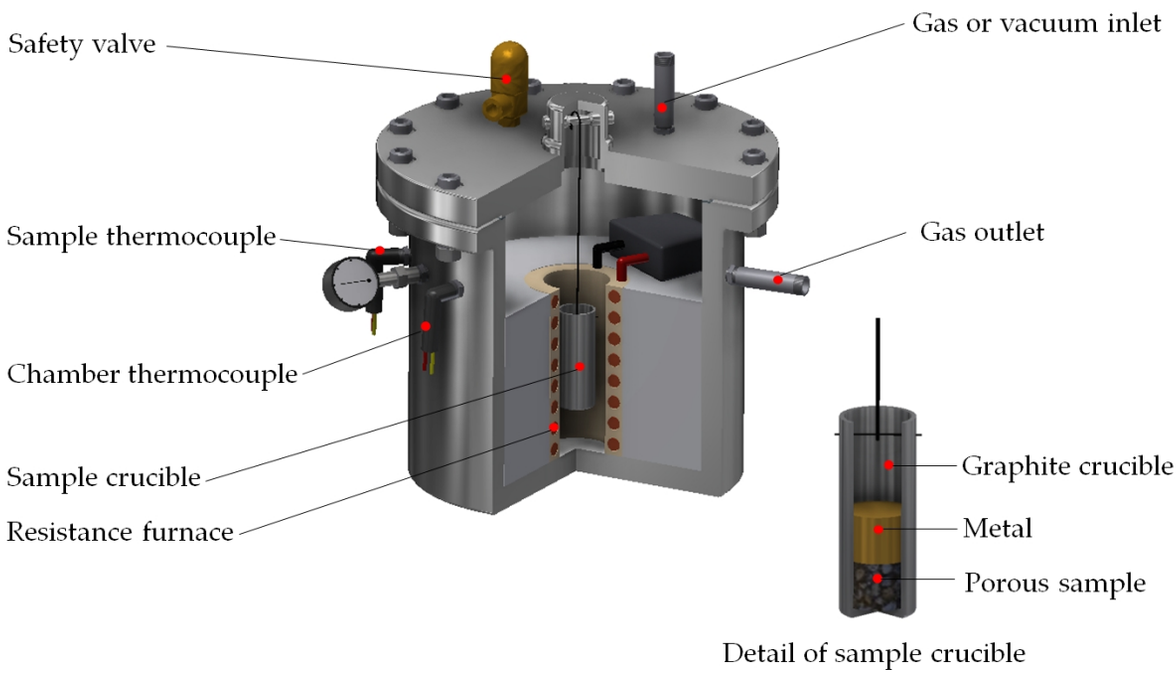

Figure 1. Schematic representation of a gas-assisted pressure infiltration (GPI) system developed at the University of Alicante and arrangement of the materials (reinforcement and matrix) inside the crucible.

At the University of Alicante, another equipment, in this case for squeeze-casting technique [30], was also developed. Figure 3 shows a schematic representation of the main body of this equipment and how it operates. The main feature of this apparatus is that it can work up to 450°C and at a maximum pressure of 150 MPa. To resist these operating conditions, special

http://dx.doi.org/10.5772/61167

(W720 Bölher) steel was used to build the body of the equipment. Embedded resistances in the central body heat the system, and temperature is measured and controlled by K type thermocouples connected to a temperature controller.

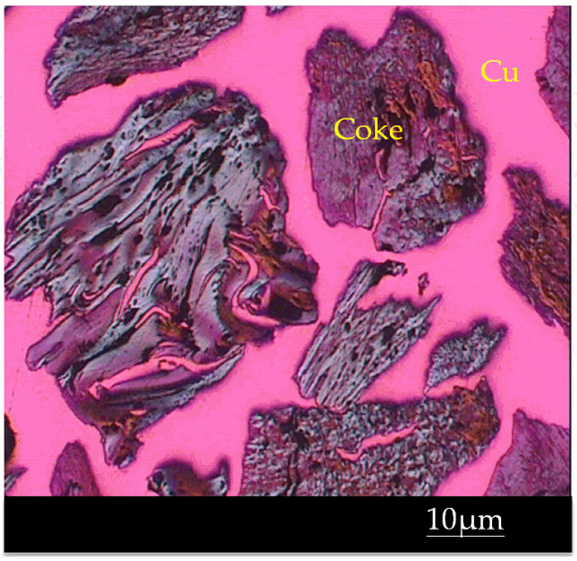

Figure 2. Polarized light optical microscopy image of a composite material obtained by GPI. The composite material consists of needle coke (reinforcement) and copper (matrix).

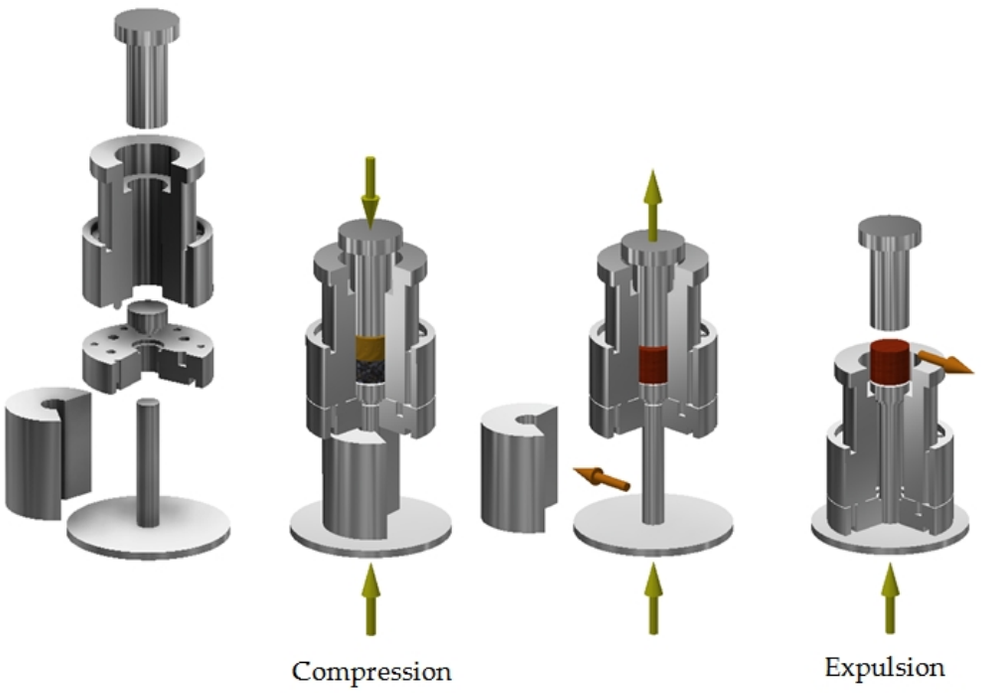

Figure 3. Schematic representation of a squeeze-casting (SC) system developed at the University of Alicante. The operating mode is indicated in the figure.

The manufacturing process of a composite material using SC can be described as follows: The system is first preheated to the operating temperature (between 350 and 450 °C depending on the alloy) to avoid early solidification of the metal matrix during infiltration. The preform is preheated (600 to 700°C) and the alloy is melted (150°C above the melting point) in two auxiliary furnaces. Thereafter, the preform is transferred to the main chamber, and the liquid metal is added. The desired pressure is applied as indicated in Figure 3. After infiltration, the system is cooled down and the manufactured material is removed as indicated in Figure 3.

The main problem with this technique is that the processing is complex because the times and temperatures must be very accurate to keep the metal from solidifying before penetrating into the preform. This disadvantage is also an advantage, since the high velocity of the process generates a finer microstructure and thus improves the mechanical properties of the final material.

Most importantly, it is possible to find in the market, both SC and GPI fully automated devices, but the basic operating principles are the same for the ones developed at University of Alicante with a scale factor between 2 and 10.

3. Wetting basic laws

One of the most relevant characteristics for the production of MMC through liquid processing routes is the wetting of the reinforcement by the liquid metals, which is quantified by measuring the contact angle between the reinforcement and matrix [31]. The contact angle between a flat substrate and a drop of liquid metal can be routinely measured by the method of the sessile drop. However, this measurement is not possible when the solid is in particulate form, in which case the wetting can be studied by means of liquid metal infiltration into compacted particulate samples [10, 11, 21-29].

Considering a solid, flat, non-deformable and chemically homogeneous surface in contact with a nonreactive liquid in the presence of a gaseous phase, if the liquid does not completely cover the solid, the liquid will form with the solid a contact angle θ, as depicted in Figure 4.

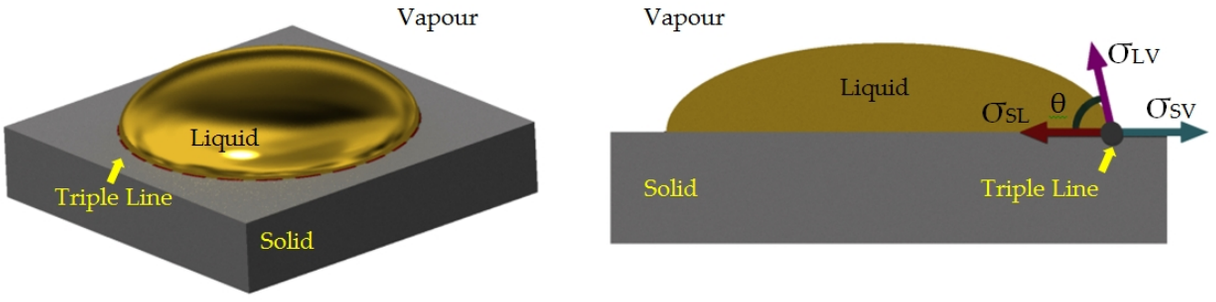

Figure 4. Configuration of a sessile drop on a substrate within which it forms a contact angle θ.

http://dx.doi.org/10.5772/61167

The equilibrium value of θ, which is used to define the wetting behavior of a fluid, can be written in terms of the balance of three energies present in the interfacial vapor-liquid-solid system, according to the well-known Young equation (1805):

$$cos\theta = \frac{\sigma_{sv} - \sigma_{sl}}{\sigma_{lv}} \tag{1}$$

where σ_{ij} is the interfacial energy between the phases *i* and *j* (s, l, and v represent the solid, liquid, and vapor phases, respectively). A contact angle of less than 90° identifies a liquid that wets the substrate, while larger angles identify liquids that do not wet it. An ideal wetting liquid will have an assigned value of θ equal to 0°.

The interfacial energy σ_{lv}, also called surface tension (γ_{lv}), can be measured with sufficient accuracy by a large number of techniques, e.g., maximum bubble pressure [32, 33], pendant drop [34], or great crucible [35, 36]. However, the surface energy of the solid-vapor phase (σ_{sv}) and the solid-liquid (σ_{sl}) phase can only be estimated. Consequently, the two variables that are unknown in the Young's equation can be grouped into only one, called work of adhesion (W_a), which expresses the strength of the solid-liquid bonds and was introduced by Dupré (1869):

$$W_a = \sigma_{lv} + \sigma_{sv} - \sigma_{sl} \tag{2}$$

If now this equation is inserted in the Young's equation, the so-called Young-Dupré equation is obtained:

$$W_a = \gamma_{lv} \cdot (1 + \cos\theta) \tag{3}$$

All infiltration processes are driven by a differential pressure that allows the liquid matrix to penetrate into the porous reinforcement. This difference of pressure between the two fluids (liquid matrix and gas phase filling porosity) is defined as the capillary pressure (P_c) and described by the famous Young-Laplace equation for a straight circular capillary:

$$\Delta P_c = P_A - P_B = \frac{2 \cdot \gamma_{lv} \cdot cos\theta}{r} \tag{4}$$

Where γ_{lv} is the liquid-vapour surface tension, θ the contact angle, and r the capillary radius. Figure 5 schematizes different infiltration situations based on the wetting or non-wetting behavior of the system.

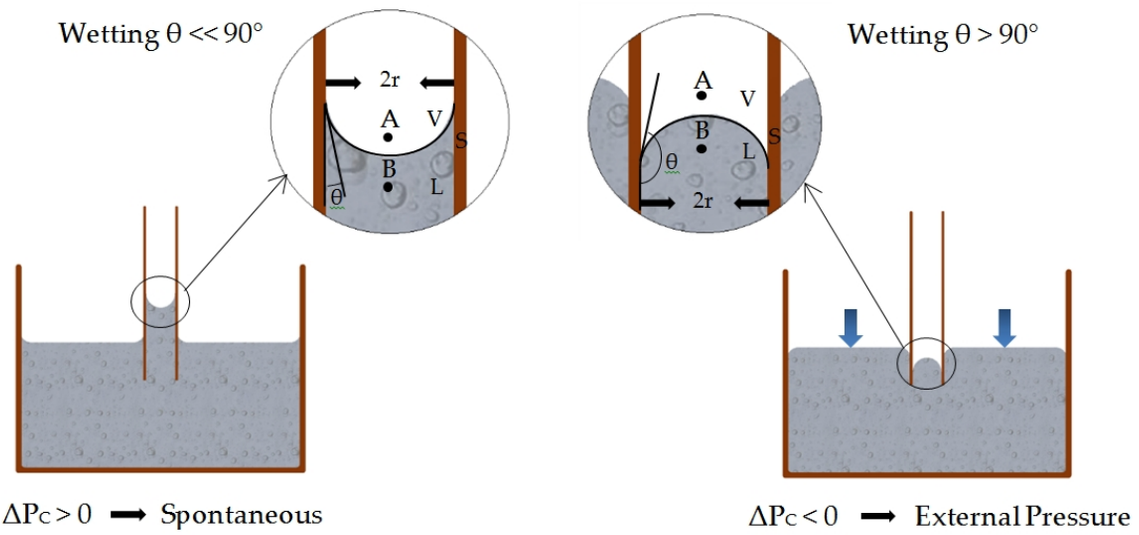

Figure 5. Scheme of infiltration process for different wetting behaving systems.

The energy shift that occurs when immersing the capillary into a liquid can be described in terms of work as:

$$W_i = \sigma_{sl} - \sigma_{sv} \tag{5}$$

where W_i is the work of immersion. For wetting systems (W_i<0), infiltration proceeds spontaneously without the necessity of applying an external pressure, as is the case of infiltration of silicon into carbon in the RBSC method. For non-wetting systems (W_i>0), infiltration does not occur unless an external pressure, superior to the threshold pressure, is applied. The threshold pressure can be written in terms of work of immersion as:

$$P_0 = S_i \cdot W_i \tag{6}$$

where S_i is the particle surface area per unit of volume of liquid matrix. Since $\sigma_{sv} = \sigma_{sl} - \gamma_{lv} \cdot cos\theta$, The threshold pressure can be related to the contact angle as:

$$P_0 = S_i \cdot \gamma_{lv} \cdot cos\theta \tag{7}$$

Since the measurement of the surface area of the particles becomes rather inaccurate when the particle diameter surpasses a certain value, and the surface roughness is very difficult to estimate, it is possible to assume a particular geometry for the porous media, e.g., cylindrical pores with a radius r as an approximation, in which case the surface area can be written as $S_i = \frac{2 \cdot \lambda \cdot (1-\phi)}{\phi \cdot r}$ and the threshold pressure can be written as:

http://dx.doi.org/10.5772/61167

$$P_0 = 2 \cdot \lambda \cdot \gamma_{lv} \cdot \cos\theta \cdot \frac{(1-\phi)}{\phi \cdot r} \tag{8}$$

Where λ is a geometrical factor introduced to describe deviation from the assumed geometry of the pores and the surface roughness of the material (it usually oscillates between 2 and 4 [10, 21-23, 25, 29], γ_{lv} is the surface tension, ϕ the porosity of the sample, r the mean pore radius, and θ is the contact angle at the triple line. It is important to emphasize that the contact angle in eq. 5 is the equilibrium contact angle that can be measured with high accuracy in sessile drop experiments.

4. The simplest case: Obtaining Darcy's law

As previously mentioned, Darcy's law predicts how a fluid moves through a porous system. This empirical law is based on the study of water movement in sand beds, and represents an ideal model in the manufacture of a composite material. Darcy's law can be derived from the resolution of the Navier-Stokes equation, considering the ideality of the system. In this section, the basis for describing the process of manufacturing of composite materials will be provided, and the most important factors that affect the process will be identified.

As aforementioned, the flow of viscous liquids is governed by the Navier-Stokes equation. This differential equation does not have a general solution. However, in some cases, it is possible to solve, e.g., for an incompressible fluid, in laminar flow (low Reynolds number), assuming that the time derivative of the fluid velocity is much smaller than its spatial derivatives, and that the effect of gravity is negligible. In this case, the equation can be reduced to:

$$\nabla P = \eta \cdot \nabla^2 v \tag{9}$$

where v is the speed of the fluid, η is the dynamic viscosity, and P the pressure. Assuming unidirectional flow (which is not so realistic in a standard porous system), it is possible to reduce the expression to the Darcy's law. This equation can be rewritten in the most commonly used form to analyze the flow of incompressible fluids through porous media:

$$v_0 = -\frac{K}{\eta} \cdot \frac{dP}{dz} \tag{10}$$

where z is the flow direction, v_0 the average superficial velocity of the fluid, dP/dz the pressure gradient along the infiltration front, and K the permeability of the porous media. The superficial velocity v_0 can be converted into infiltration velocity (dz/dt) in the porous medium by means of the porosity ϕ:

$$v_0 = \phi \cdot \frac{dz}{dt} \tag{11}$$

Combining both equations and integrating, the Darcy's law, which shows the relationship between infiltration distance (h), time (t) and the pressure drop in the infiltrating liquid (ΔP=P-Po) is obtained.

$$h^2 = \frac{2 \cdot K \cdot t}{\eta \cdot \phi} \cdot \Delta P \tag{12}$$

It must be pointed out that the permeability of the porous media is proportional to the square of the average pore radius:

$$K = a \cdot r^2 \tag{13}$$

Darcy's law has been widely used in basic studies of manufacture of metal matrix composites. Despite its simplicity, it has proven to be very useful in metallurgical engineering. As an example, the results of infiltration of liquid aluminium into a porous bed of particles, obtained by Narciso et al., are shown in Figure 6 [10, 25]. Figure 6a provides the relationship between infiltration distance and applied pressure for liquid aluminium into a porous bed of alumina particles, while Figure 6b shows the results for a liquid infiltration of an aluminium alloy into preforms of graphite particles. As predicted by Darcy's law, the square of infiltration distance is proportional to the pressure drop (h^2 vs ΔP) in these systems.

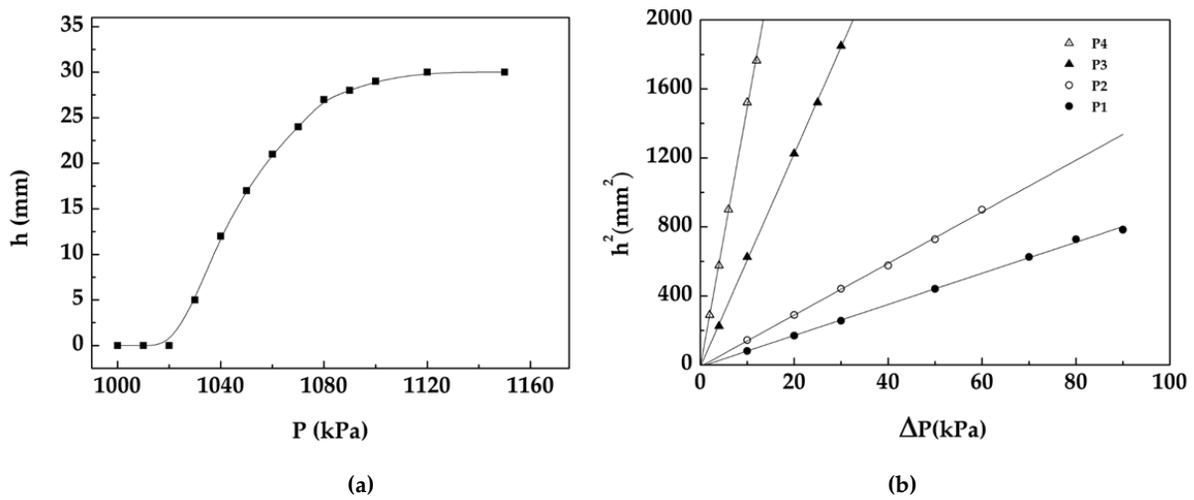

Figure 6. Evolution of the infiltrated height as a function of pressure for liquid aluminium on a preform of alumina particles (Alumina particles AA10, Vp = 59 %, Temperature = 700 °C) (a). Evolution of the square of the infiltrated height for a liquid aluminium alloy as a function of pressure drop on a preform of carbon particles at temperature of 700 °C (see the appendix for the characteristics of the graphite particles) (b).

http://dx.doi.org/10.5772/61167

As discussed in the preceding paragraphs, to solve the Navier-Stokes equation a full saturation and a laminar flow (Re < 2100) have been assumed. Besides, the effect of gravity has been considered to be negligible. Figure 6b shows a good correlation of the experimental data with Darcy's law, and thus, the assumed conditions should be valid. Reynolds number (Re) can be obtained from the following expression:

$$Re = \frac{\rho \cdot v \cdot D}{\eta} \tag{14}$$

Where ρ is the density of the liquid metal; D is the diameter of the channel, which in this case is the interparticle distance that can be assumed to be about 1/3 of the average size of the particles; v is the fluid velocity, which is comprised between 1 and 5 mm/s (in our equipments); and η the dynamic fluid viscosity. If the Reynolds number is calculated for the experiments shown in Figure 6, the values obtained are between 0.001 and 0.7, which means that the laminar flow assumption is indeed correct. The force exerted by gravity would be the metallostatic pressure of the melt, which is given by:

$$P = \rho \cdot g \cdot h \tag{15}$$

And considering that the liquid column is always less than 10 cm, in the case of aluminium for example, the pressure would be about 2 kPa, which is almost 3 orders of magnitude lower than the capillary forces, and therefore negligible.

In the following sections different real situations that can occur are considered and will be analyzed separately. The combination of all these particular cases simultaneously, although more realistic, is much more complex and goes beyond the scope of this chapter.

5. The effect of saturation

On systems where the liquid does not wet the solid, which is most common in MMCs, it must be taken into account that the permeability of the porous system is not constant [37-39] and that it depends on the saturation and this latter, and at the same time, on the applied pressure [21, 40-42].

The study of unsaturated flow is well known in geology and in 1931 it was described mathematically by Richards [34], whose partial differential equations are difficult to solve and usually solved numerically for each particular case. Numerous researchers have worked on this particular hydrodynamics and mathematical problem [44,45], and the books by Prof. Bear collect these study cases [46-48], which are essential reading for researchers working in this field. It is also noteworthy that Prof. Bear highlights in his books the goodness of Darcy's law, and that its application range is wider (more useful) than it was expected at first (i.e., unsaturated flow, high Reynolds number, etc.).

These studies were not limited to the case study of hydrology, but have crossed over to the field of metal matrix composites (MMC), performed especially by the group of Andreas Mortensen [40-42], but as mentioned above without analytical solution of the differential equations describing the phenomenon. The highlight to be found in the recent literature are two articles that show that close to the threshold pressure, infiltration is actually governed by percolation phenomena (instead of slug flow) [49,50].

Another aspect to consider is that pressure also depends on the position along the flow path, and is usually assumed that the pressure drop between the front (P_0) and head (applied pressure) is linear, which is reasonably sane. Nevertheless, in order for the differential equations to have an analytic solution, it will be assumed in this chapter that practically all the preform is at the same pressure, which in principle is something reasonable as working pressures oscillate between 1 and 5% of the threshold pressure (i.e., head=$1.05P_0$; front=P_0).

In the literature, several models showing the relationship between pressure and saturation have been described, but the most famous are the Brooks-Corey (BC) [19] and van Genuchten (VG) [20] models. In this section, the Navier-Stokes equation has been solved considering that the permeability is not constant, relating it to the saturation through the BC and VG models. Different authors have used these models to describe the infiltration process in MMCs [51]. However, previous works have shown that for low pressures (close to the threshold pressure) these models, especially the BC, do not describe the infiltration process correctly [52, 53].

Starting from reduced Navier-Stokes equation:

$$dz^2 = \frac{K \cdot t}{\eta \cdot \varnothing} \cdot dP \tag{16}$$

Where z is the infiltration distance, K the permeability, t the time of infiltration, η the dynamic viscosity of the fluid, $\varnothing$ the porosity of the porous body, and P the applied pressure. Permeability can be decomposed into two different terms, intrinsic permeability (K_i), which depends exclusively on the nature of the solid phase; and relative permeability (K_r), which depends on the degree of saturation (S) of the system:

$$K = K_i \cdot K_r \tag{17}$$

Relative permeability, depends on the degree of saturation according to:

$$K_r = S^n \tag{18}$$

Where n is a parameter that ranges from 1 to 3. In the case of composites fabricated by infiltration, it has been found that 1 is the most accurate value for n [51]. There are several models that relate saturation to the applied pressure (P) and the threshold pressure (P_0) of the system. One of the most used models of this kind is the Brooks-Corey equation:

http://dx.doi.org/10.5772/61167

$$S = 1 - \left(\frac{P_0}{P} \right)^{\lambda} \tag{19}$$

Where λ is a parameter that depends on the solid material. Replacing K in eq. 16 with eqs. 17, 18, and 19 yields a modified reduced Navier-Stokes equation:

$$dz^2 = \frac{K_i \cdot \left[1 - \left(\frac{P_0}{P} \right)^{\lambda} \right]^n \cdot t}{\eta \cdot \varnothing} \cdot dP \tag{20}$$

Solving this equation provides a model to estimate depth of infiltration as a function of applied pressure. In this form, there is no general analytical solution to the equation, so, to obtain an analytical model, a particular case must be considered. As discussed above, experimental data fit better when $n = 1$, so to solve the equation, this particular case will be considered:

$$\frac{1}{2} \cdot h^2 = \frac{K_i \cdot t}{\eta \cdot \varnothing} \int \left(1 - \left(\frac{P_0}{P} \right)^{\lambda} \right) \cdot dP \tag{21}$$

$$h^2 = \frac{2 \cdot K_i \cdot t}{\eta \cdot \varnothing} \cdot \left(P + \frac{P \cdot \left(\frac{P_0}{P} \right)^{\lambda}}{\lambda - 1} + A \right) \tag{22}$$

Where A is the integration constant, and its value can be determined using initial conditions, i.e., for $P = P_0$ and $h = 0$

$$0 = \frac{2 \cdot K_i \cdot t}{\eta \cdot \varnothing} \cdot \left(P_0 + \frac{P_0 \cdot \left(\frac{P_0}{P_0} \right)^{\lambda}}{\lambda - 1} + A \right) \tag{23}$$

$$\begin{aligned} 0 &= P_0 + \frac{P_0}{\lambda - 1} + A \\ A &= -P_0 - \frac{P_0}{\lambda - 1} \\ & P_0 \cdot \left(-\frac{1}{\lambda - 1} - 1 \right) \end{aligned} \tag{24}$$

Then the final expression for $h(P)$ is:

$$h^2 = \frac{2 \cdot K_i \cdot t}{\eta \cdot \varnothing} \cdot \left(P + \frac{P \cdot \left(\frac{P_0}{P} \right)^{\lambda}}{\lambda - 1} - P_0 \cdot \left(\frac{1}{\lambda - 1} + 1 \right) \right) \tag{25}$$

It must be noted that if λ acquires a very high value, the model tends to Darcy's law:

$$\lambda \to \infty$$

$$h^2 = \frac{2 \cdot K_i \cdot t}{\eta \cdot \varnothing} \cdot \left(P + 0 - P_0 \cdot \left(0 + 1 \right) \right)$$

$$h^2 = \frac{2 \cdot K_i \cdot t}{\eta \cdot \varnothing} \cdot \left(P - P_0 \right)$$

If, instead of using the Brooks-Corey equation, the Van Genuchten model is applied:

$$S = 1 - \left[1 + (\alpha \cdot (P - P_0))^{n1} \right]^{-m} \tag{26}$$

$$m = 1 - \frac{1}{n1} \tag{27}$$

where α is a scale parameter inversely proportional to the mean pore diameter, and $n1$ (called n1 to differentiate from n in eq. 18) and m are shape parameters. The reduced Navier-Stokes equation results in:

$$dz^2 = \frac{K_i \cdot \left[1 - \left[1 + \alpha \cdot (P - P_0)^{n1} \right]^{-1 + \frac{1}{n1}} \right]^{n} \cdot t}{\eta \cdot \varnothing} \cdot dP \tag{28}$$

As in the case of the Brooks-Corey model, a general analytical solution is not available, so the case of n = 1 will be considered again:

$$dz^2 = \frac{K_i \cdot \left[1 - \left[1 + \alpha \cdot (P - P_0)^{n1} \right]^{-1 + \frac{1}{n1}} \right] \cdot t}{\eta \cdot \varnothing} \cdot dP \tag{29}$$

http://dx.doi.org/10.5772/61167

$$\frac{1}{2}\cdot h^2 = \frac{K_i\cdot t}{\eta\cdot\varnothing}\cdot\int\left[1-\left[1+(\alpha\cdot(P-P_0))^{n1}\right]^{-1+\frac{1}{n1}}\right]\cdot dP \tag{30}$$

$$\frac{1}{2}\cdot h^2 = \frac{K_i\cdot t}{\eta\cdot\varnothing}\cdot\int 1\cdot dP - \int\left[1+(\alpha\cdot(P-P_0))^{n1}\right]^{-1+\frac{1}{n1}}\cdot dP \tag{31}$$

$$\frac{1}{2}\cdot h^2 = \frac{K_i\cdot t}{\eta\cdot\varnothing}\cdot P - \int\left[1+(\alpha\cdot(P-P_0))^{n1}\right]^{-1+\frac{1}{n1}} dP \tag{32}$$

.

The second integral does not have an analytical solution either, so in order to obtain a solution as general as possible, the value of n1=2 is introduced [42, 51]:

$$h^2 = \frac{2\cdot K_i\cdot t}{\eta\cdot\varnothing}\cdot\left[P-\int\left[1+(\alpha\cdot\left(P-P_0\right))^2\right]^{-1/2} dP\right] \tag{33}$$

$$\frac{1}{2}\cdot h^2 = \frac{2\cdot K_i\cdot t}{\eta\cdot\varnothing}\cdot\left[P-\int\frac{1}{\sqrt{1+(\alpha\cdot(P-P_0))^2}}dP\right] \tag{34}$$

Applying the substitution $u=\alpha\cdot(P-P_0)$, $du=\alpha\cdot dP$ results in:

$$h^2 = \frac{2\cdot K_i\cdot t}{\eta\cdot\varnothing}\cdot\left[P-\int\frac{1}{\sqrt{1+u^2}}\cdot\frac{1}{\alpha}\cdot du\right] \tag{35}$$

$$h^2 = \frac{2\cdot K_i\cdot t}{\eta\cdot\varnothing}\cdot\left[P-\frac{1}{\alpha}\cdot\int\frac{1}{\sqrt{1+u^2}}\cdot du\right] \tag{36}$$

$$h^2 = \frac{2\cdot K_i\cdot t}{\eta\cdot\varnothing}\cdot\left[P-\frac{\operatorname{arcsinh}\left(u\right)}{\alpha}\cdot+C\right] \tag{37}$$

Replacing back $u=\alpha\cdot(P-P_0)$:

$$h^2 = \frac{2 \cdot K_i \cdot t}{\eta \cdot \varnothing} \cdot \left[P - \frac{\operatorname{arcsinh}\left(\alpha \cdot (P - P_0)\right)}{\alpha} + C \right] \tag{38}$$

To estimate the value of C, initial conditions must be applied $P = P_0$ and $h = 0$.

$$0 = \frac{2 \cdot K_i \cdot t}{\eta \cdot \varnothing} \cdot \left[P_0 - \frac{\operatorname{arcsinh}\left(0\right)}{\alpha} \cdot + C \right] \tag{39}$$

$$C = -P_0 \tag{40}$$

Then, the general solution for n1 = 2 is:

$$h^2 = \frac{2 \cdot K_i \cdot t}{\eta \cdot \varnothing} \cdot \left[(P - P_0) - \frac{\operatorname{arcsinh}\left(\alpha \cdot (P - P_0)\right)}{\alpha} \right] \tag{41}$$

In order to analyze the accuracy of the results, the evolution of the square of the infiltrated height as a function of pressure drop is plotted in Figures 7a and 7b. As shown, experimental results are perfectly framed between the line defined by Darcy's law (assuming that the liquid permeability is invariant and therefore permeability measured with polyethylene glycol is used) and the curve modified with the Van Genuchten equation.

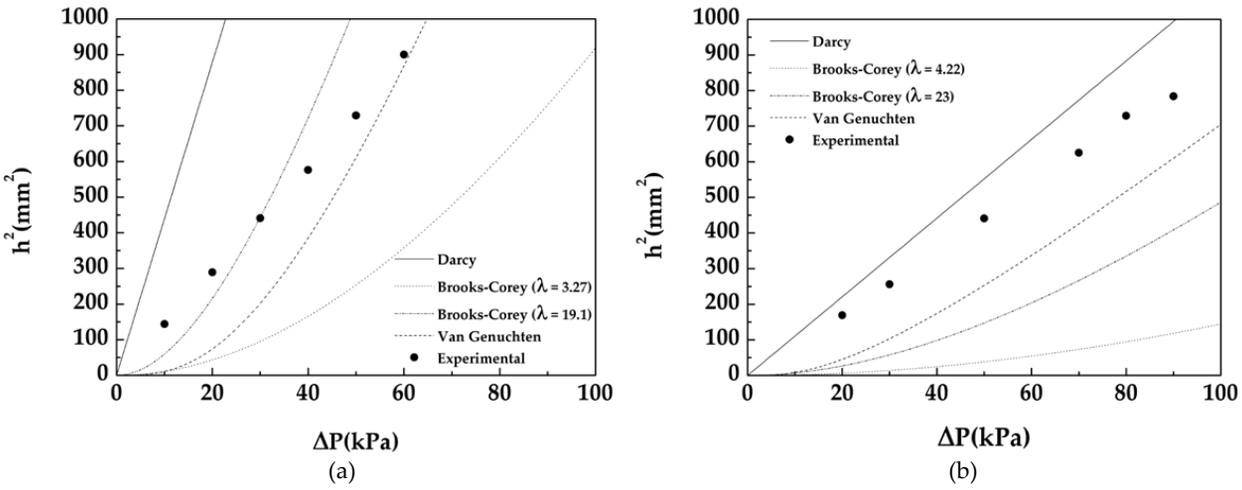

Figure 7. Evolution of the square of infiltrated height for liquid aluminium-silicon alloy as a function of pressure drop on a preform of graphite particles P1 at 700°C) (a). Evolution of the square of the infiltrated height for liquid aluminium-silicon alloy as a function of pressure drop on a preform of carbon particles P2 at 700°C) (b) Characteristics of the graphite particles are listed in the appendix. The coefficients for the BC model have been extracted from [53].

http://dx.doi.org/10.5772/61167

The results shown here clearly demonstrate that it is not necessary to solve the Richards equation (modified Darcy's law to take into account saturation), which has only numerical solutions to predict infiltration in composite materials unlike what was suggested by Mortensen et al. [54]. It is noteworthy that many authors in soil mechanics indicate that Darcy's law is more universal than it was originally supposed.

6. The effect of variable radius

Although the variation of the radius is not a very common phenomenon in the manufacture of composite materials, it is a process that can occur. The variation of the radius is a fundamental issue for example in the manufacture of SiC by the RBSC process or reactive infiltration and SiC derived CMCs. This is a rather complex situation since the variation of the radius affects the permeability of the porous media.

To solve the Navier-Stokes equation it has been assumed that the reduction of the radius, caused by a chemical reaction, is controlled by diffusion. The equations presented so far are valid for infiltration in nonreactive systems. However, they are not valid for reactive infiltration because the pore radius, in this kind of systems, is not constant but decreases with the generation of new solid. As discussed above, the threshold pressure and the permeability depend on the radius, so they are not invariant over time.

So for reactive systems, it is necessary to re-solve the reduced Navier-Stokes equation considering the variation of the radius:

$$\phi \cdot \frac{dz}{dt} = -\frac{K}{\eta} \cdot \frac{dP}{dz} \tag{42}$$

After integration, the following expression is obtained:

$$\frac{1}{2}h^2 = -\frac{K}{\varnothing \cdot \eta} dP \cdot dt \tag{43}$$

Usually in reactive systems, infiltration takes place spontaneously (without applying an external pressure), so $\Delta P = P_0$. Differentiating the expression for P_0 results in:

$$\mathrm{dP} = -2 \cdot \lambda \cdot \gamma_{lv} \cdot cos\theta \cdot \frac{(1-\phi)}{\Phi \cdot r^2} \cdot dr \tag{44}$$

Combining this expression with eq. 6 yields:

$$\frac{1}{2}\cdot h^2 = - \quad \frac{a\cdot r^2}{\varnothing\cdot\eta}\left(-2\cdot\lambda\cdot\gamma_{lv}\cdot cos\theta\cdot\frac{(1-\phi)}{\varnothing\cdot r^2}\right)\cdot dr\cdot dt \tag{45}$$

Simplifying and rearranging:

$$h^2 = 4\cdot\lambda\cdot a\cdot\gamma_{lv}\cdot cos\theta\cdot\frac{(1-\phi)}{\eta\cdot\varnothing^2}\cdot \quad dr\cdot dt \tag{46}$$

In principle, porosity of the system is not constant, but for a first approximation it can be considered so. To proceed with the solution of the equation, a relationship between radius and time is necessary. Assuming that the controlling step of the reaction is the diffusion of C through the SiC layer, then the model of decreasing nucleus developed in the decade of the 1950s can be used [55, 56]:

$$t = \frac{M_{Si}\cdot\rho_{SiC}\cdot r_o^2}{6\cdot M_{SiC}\cdot\mathcal{D}_{C/SiC}\cdot\rho_{Si}}\left[1-3\cdot\left(\frac{r}{r_o}\right)^2+2\cdot\left(\frac{r}{r_o}\right)^3\right] \tag{47}$$

$$dt = \frac{M_{Si}\cdot\rho_{SiC}\cdot r_o^2}{6\cdot M_{SiC}\cdot\mathcal{D}_{C/SiC}\cdot\rho_{Si}}\cdot\left[-6\cdot\left(\frac{r}{r_o^2}\right)+6\cdot\left(\frac{2r^2}{r_o^3}\right)\right]\cdot dr \tag{48}$$

Where ρ_{SiC} is the density of SiC, r_0 the initial pore radius, $D_{C/SiC}$ the diffusion coefficient of C atoms through SiC, and ρ_{Si} the density of Si atoms in kg/m^3, M_{SiC} and M_{Si} the molar weight of SiC and Si, respectively.

Introducing these relations into eq. 46 and defining:

$$G = 4\cdot\lambda\cdot a\cdot\gamma_{lv}\cdot cos\theta\cdot\frac{(1-\phi)}{\eta\cdot\varnothing^2}\frac{M_{Si}\cdot\rho_{SiC}\cdot r_o^2}{6\cdot\mathcal{D}_{C,SiC}\cdot M_{SiC}\cdot\rho_{Si}} \tag{49}$$

Results in the following expression:

$$h^2 = G\cdot \quad \left[-6\cdot\left(\frac{r}{r_o^2}\right)+6\cdot\left(\frac{r^2}{r_o^3}\right)\right]dr\cdot dr \tag{50}$$

Solving the first integral yields:

http://dx.doi.org/10.5772/61167

$$h^2 = G\cdot\int_0^r\left[A - 3\cdot\left(\frac{r}{r_o}\right)^2 + 2\cdot\left(\frac{r}{r_o}\right)^3\right]\cdot dr \tag{51}$$

Where A is an integration constant. Solving the second integral results in:

$$h^2 = G\cdot\left(A\cdot r - \left(\frac{r^3}{r_o^2}\right) + \frac{1}{2}\cdot\left(\frac{r^4}{r_o^3}\right) + B\right) \tag{52}$$

where B is an integration constant. In order to obtain the final solution, boundary conditions must be used to find the values of A and B:

a. $r = r_o \rightarrow h = 0 \rightarrow t = 0$

b. $r = 0 \rightarrow h = h_{MAX} \rightarrow t = \tau \rightarrow \frac{dh}{dr} = 0$

Where $\tau = \frac{M_{Si}\cdot\rho_{SiC}\cdot r_o^2}{6\cdot M_{SiC}\cdot\mathcal{D}_{C/SiC}\cdot C_{Si}}$

By applying condition a), the next expression is obtained:

$$0 = G\cdot\left(A\cdot r_0 - \left(\frac{r_0^3}{r_o^2}\right) + \frac{1}{2}\cdot\left(\frac{r_o^4}{r_o^3}\right) + B\right) \tag{53}$$

Applying condition b) leads to:

$$h_{MAX}^2 = G\cdot B \tag{54}$$

and

$$\frac{dh}{dr} = 0 = \frac{G\cdot\left(A - 6\cdot\left(\frac{r^2}{r_o^2}\right) + 2\cdot\left(\frac{r^3}{r_o^3}\right)\right)}{2\sqrt{G\cdot\left(A\cdot r - \left(\frac{r^3}{r_o^2}\right) + \frac{1}{2}\cdot\left(\frac{r^4}{r_o^3}\right) + B\right)}} \tag{55}$$

Solving eq. 55 leads to:

$$A = 0$$

Replacing the value of A in eq. 53 results in:

$$B = \frac{1}{2} \cdot r_0$$

Replacing the value of B in eq. 54 provides the expression for h_{MAX}:

$$h_{MAX} = \sqrt{\lambda \cdot a \cdot \gamma_{lv} \cdot cos\theta \cdot \frac{(1-\phi)}{\eta \cdot \varnothing^2} \cdot \frac{M_{Si} \cdot \rho_{SiC} \cdot r_o^3}{3 \cdot \mathcal{D}_{C,SiC} \cdot M_{SiC} \cdot \rho_{Si}}} \tag{56}$$

And after replacing the values of A and B, and rearranging the final expression h(r) is obtained:

$$h^2 = \lambda \cdot a \cdot \gamma_{lv} \cdot cos\theta \cdot \frac{(1-\phi)}{\eta \cdot \varnothing^2} \cdot \frac{\rho_{SiC} \cdot r_o^2 \cdot r}{3 \cdot \mathcal{D}_{C,SiC} \cdot \rho_{Si}} \cdot \left[\left(\frac{r}{r_0} \right)^3 - 2 \cdot \left(\frac{r}{r_0} \right)^2 + \frac{r_0}{r} \right] \tag{57}$$

$$h^2 = \frac{h_{MAX}^2}{r_0} \cdot r \cdot \left[\left(\frac{r}{r_0} \right)^3 - 2 \cdot \left(\frac{r}{r_0} \right)^2 + \frac{r_0}{r} \right] \tag{58}$$

$$h^2 = h_{MAX}^2 \cdot \left[\left(\frac{r}{r_0} \right)^4 - 2 \cdot \left(\frac{r}{r_0} \right)^3 + 1 \right] \tag{59}$$

It must be taken into consideration that this equation is valid only as long as the modification of the porosity is negligible. For evaluating h(t), eq. 59 and eq. 47 must be combined.

Figure 8 shows the calculated infiltration distance with time for a carbon preform with an initial pore radius of 30 micron and 50% open porosity, infiltrated with pure Si, using Darcy's law and the variable radius model for cylindrical and spherical pores. The variable radius models predict a slower rate of infiltration, which is closer to the experimental data obtained by several authors [12, 57-61].

Another approach is to consider that the pore closure is limited by the chemical reaction that originates it. In this case, the equations of the decreasing nucleus model to be used are:

$$t = \frac{M_{Si} \cdot \rho_{SiC} \cdot r_0}{k_s \cdot \rho_{Si} \cdot M_{SiC}} \cdot \left(1 - \frac{r}{r_0} \right) \tag{60}$$

http://dx.doi.org/10.5772/61167

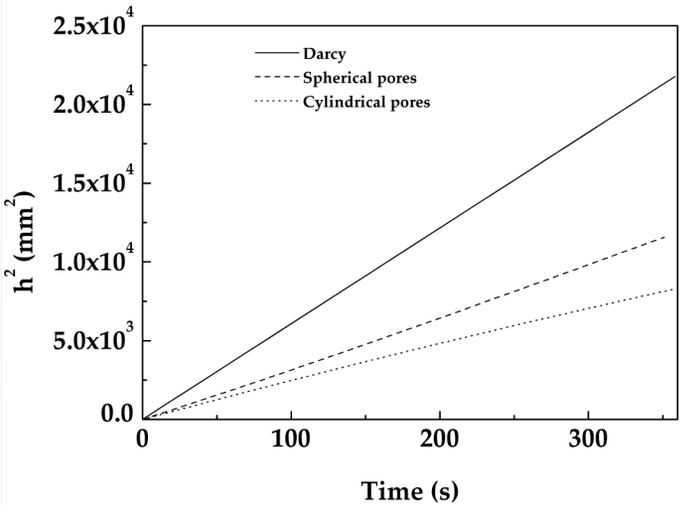

Figure 8. Comparison of the square distance of infiltration (h^2) vs. time, calculated using Darcy's law and variable radius models for a carbon with an initial pore radius of 30 micron, and 50% porosity, infiltrated with pure Si. For the variable radius model, the pore closure is assumed to be controlled by diffusion, and two different pore geometries are considered. Infiltration is simulated until the pore radius decreases by 30%.

$$dt = -\frac{\rho_{SiC}}{k_s \cdot \rho_{Si}} \cdot dr \tag{61}$$

Introducing this equation into the reduced Navier-Stokes equation and solving the integrals results in:

$$h^2 = -4 \cdot \lambda \cdot a \cdot \gamma_{lv} \cdot \cos\theta \cdot \frac{(1-\phi)}{\eta \cdot \varnothing^2} \cdot \frac{M_{Si} \cdot \rho_{SiC}}{k_s \cdot \rho_{Si} \cdot M_{SiC}} \cdot \int (r + A) \cdot dr \tag{62}$$

$$h^2 = -4 \cdot \lambda \cdot a \cdot \gamma_{lv} \cdot \cos\theta \cdot \frac{(1-\phi)}{\eta \cdot \varnothing^2} \cdot \frac{M_{Si} \cdot \rho_{SiC}}{k_s \cdot \rho_{Si} \cdot M_{SiC}} \cdot \left(\frac{r^2}{2} + A \cdot r + B \right) \tag{63}$$

The integration constants A and B are calculated using contour conditions:

c. $r = r_o \rightarrow h = 0 \rightarrow t = 0$

d. $r = 0 \rightarrow h = h_{MAX} \rightarrow t = \tau \rightarrow dh / dr = 0$

a. For condition a):

$$0 = -4 \cdot \lambda \cdot a \cdot \gamma_{lv} \cdot \cos\theta \cdot \frac{(1-\phi)}{\eta \cdot \varnothing^2} \cdot \frac{M_{Si} \cdot \rho_{SiC}}{k_s \cdot \rho_{Si} \cdot M_{SiC}} \cdot \left(\frac{r_0^2}{2} + A \cdot r_0 + B \right) \tag{64}$$

For condition b):

$$\frac{dh}{dr} = 0 = \frac{-4 \cdot \lambda \cdot a \cdot \gamma_{lv} \cdot \cos\theta \cdot \frac{(1-\phi)}{\eta \cdot \varnothing^2} \cdot \frac{M_{Si} \cdot \rho_{SiC}}{k_s \cdot \rho_{Si} \cdot M_{SiC}} \cdot (0 + A)}{2 \cdot \sqrt{-4 \cdot \lambda \cdot a \cdot \gamma_{lv} \cdot \cos\theta \cdot \frac{(1-\phi)}{\eta \cdot \varnothing^2} \cdot \frac{M_{Si} \cdot \rho_{SiC}}{k_s \cdot \rho_{Si} \cdot M_{SiC}} \cdot \left(\frac{0}{2} + A \cdot 0 + B\right)}} \tag{65}$$

$$A = 0 \tag{66}$$

and replacing in condition a):

$$0 = -4 \cdot \lambda \cdot a \cdot \gamma_{lv} \cdot \cos\theta \cdot \frac{(1-\phi)}{\eta \cdot \varnothing^2} \cdot \frac{M_{Si} \cdot \rho_{SiC}}{k_s \cdot \rho_{Si} \cdot M_{SiC}} \cdot \left(\frac{r_0^2}{2} + 0 \cdot r_0 + B\right) \tag{67}$$

$$B = -\frac{r_0^2}{2} \tag{68}$$

and

$$h_{MAX} = \sqrt{\lambda \cdot a \cdot \gamma_{lv} \cdot \cos\theta \cdot \frac{(1-\phi)}{\eta \cdot \varnothing^2} \cdot \frac{M_{Si} \cdot \rho_{SiC}}{k_s \cdot \rho_{Si} \cdot M_{SiC}} \cdot r_0^2} \tag{69}$$

Replacing the values of A, B and h_{MAX}:

$$h^2 = 4 \cdot \lambda \cdot a \cdot \gamma_{lv} \cdot \cos\theta \cdot \frac{(1-\phi)}{\eta \cdot \varnothing^2} \cdot \frac{M_{Si} \cdot \rho_{SiC}}{k_s \cdot \rho_{Si} \cdot M_{SiC}} \cdot \left(\frac{r_0^2 - r^2}{2}\right) \tag{70}$$

Figure 9 shows the square of the infiltration distance as a function of time for a carbon preform with an initial pore radius of 30 micron and 50% open porosity infiltrated with pure Si, using Darcy's law and the variable radius model for a chemically controlled pore closure. As seen, infiltration rate decreases with time, just as in the previous case (diffusion controlled pore closure). However, the experimental data [12, 42, 59-66] show that the infiltration rate is lower than the one predicted by these models; furthermore, infiltrated height is proportional to t instead of to $t^{(1/2)}$. Experiments indicate that infiltration is controlled by the reaction at the triple line and not by the viscous phenomena described here. However, both interpretations are compatible. It is probable that in the first stage of the process, infiltration is controlled by the

http://dx.doi.org/10.5772/61167

reaction at the triple line, and after the SiC interface has been formed, the viscous flow becomes the controlling process. A completely different approach to the process of infiltration is performed by Sergi et al. [67, 68], in which they use Lattice-Bolztman models to describe infiltration in a single capillary and predict that infiltration distance is proportional to time when considering pore narrowing of the capillary due to the reaction. However, their predictions have not been validated experimentally up to date. It is possible to conclude that a deeper understanding of the reactive infiltration phenomenon should be gained in order to discern what is happening in the overall process.

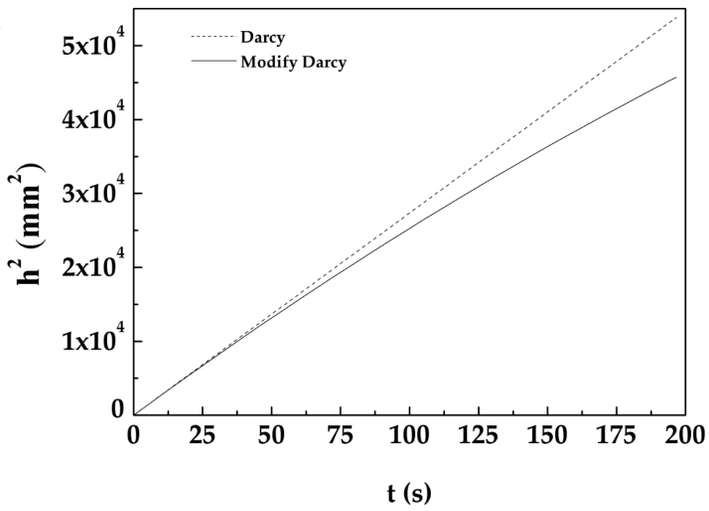

Figure 9. Comparison of the square distance of infiltration (h^2) as a function of time, calculated using Darcy's law and the variable radius models for a carbon with an initial pore radius of 30 micron, and 50% porosity, infiltrated with pure Si. For the variable radius model, pore closure is assumed to be controlled by the chemical reaction. Infiltration is simulated until the pore radius decreases by 30%.

7. Effect of variable viscosity: Curing polymeric resins

The properties of PMCs depend strongly on the type of matrix used. Among the possible binders, thermoset resins present a singularity: their viscosity is time dependent [69, 70]. These kinds of polymers present an initial low viscosity that grows exponentially with time. During this process, the material undergoes a series of chemical reactions that cause the cross-linking of polymeric chains yielding a 3D structure with excellent thermal stability and solvent resistance. The process of cross-linking that takes place in these resins is known as curing. In polymer matrix composites in which the matrix cures with time, thus hardening and losing fluidity, viscosity becomes a limiting factor in infiltration.

The evolution of viscosity is usually expressed with the following equation:

$$\eta = \eta_0 \cdot e^{k_n \cdot t} \tag{71}$$

Where η_0 is the initial viscosity and k_n is a strongly temperature-dependent rheological kinetic constant [70]. Starting from the reduced Navier-Stokes equation:

$$\phi \cdot \frac{dz}{dt} = -\frac{K}{\eta} \cdot \frac{dP}{dz} \tag{72}$$

After integration, the following expression is obtained:

$$\frac{1}{2} \cdot h^2 = - \quad \frac{K}{\varnothing \cdot \eta} dP \cdot dt \tag{73}$$

Introducing eq. 71 and solving the integral yields a model for predicting infiltration distance as a function of time for curing polymeric resins:

$$\frac{1}{2} \cdot h^2 = - \quad \frac{K}{\varnothing \cdot \eta_0 \cdot e^{k_n \cdot t}} dP \cdot dt \tag{74}$$

$$\frac{1}{2} \cdot h^2 = -\frac{K}{\varnothing \cdot \eta_0} \cdot \quad \frac{dP}{e^{k_n \cdot t}} \cdot dt \tag{75}$$

$$h^2 = -\frac{2 \cdot K \cdot \Delta P}{\varnothing \cdot \eta_0} \cdot \int e^{-k_n \cdot t} \cdot dt \tag{76}$$

$$h^2 = \frac{2 \cdot K \cdot \Delta P}{\varnothing \cdot \eta_0} \cdot \frac{e^{-k_n \cdot t}}{k_n} + A \cdot t + B \tag{77}$$

To calculate the values of integration constants A and B, initial conditions are applied:

a. $t = 0; h = 0$

b. $t = \infty; \frac{dh}{dt} = 0$

For condition a):

$$\begin{aligned} 0 &= \frac{2 \cdot K \cdot \Delta P}{\varnothing \cdot \eta_0} \cdot \frac{1}{e^{k_n \cdot 0}} + A \cdot 0 + B \\ B &= -\frac{2 \cdot K \cdot \Delta P}{\varnothing \cdot \eta_0 \cdot k_n} \end{aligned} \tag{78}$$

http://dx.doi.org/10.5772/61167

for condition b):

$$\frac{dh}{dt} = 0 = \frac{-\frac{2 \cdot K \cdot \Delta P}{\varnothing} \cdot e^{-k_n \cdot t} + A}{2 \cdot \sqrt{\cdot \frac{e^{-k_n \cdot t}}{-k_n} + A \cdot t + B}} \qquad A = 0 \tag{79}$$

Then the final equation results in:

$$h^2 = \frac{2 \cdot K \cdot \Delta P}{\varnothing \cdot \eta_0 \cdot k_n} \cdot e^{-k_n \cdot t} - \frac{2 \cdot K \cdot \Delta P}{\varnothing \cdot \eta_0 \cdot k_n} \tag{80}$$

$$h^2 = -\frac{2 \cdot K \cdot \Delta P}{\varnothing \cdot \eta_0 \cdot k_n} \cdot (1 - e^{-k_n \cdot t}) \tag{81}$$

It must be highlighted that the negative sign is only indicative of the direction of flow. Figure 10 shows the evolution of the square of infiltrated height for a preform infiltrated with curing resins with an initial viscosity of 100 Pa s at different temperatures. The drastic effect of temperature on infiltration distance becomes evident, since increasing temperature to 50°C reduces infiltrated distance by one order of magnitude.

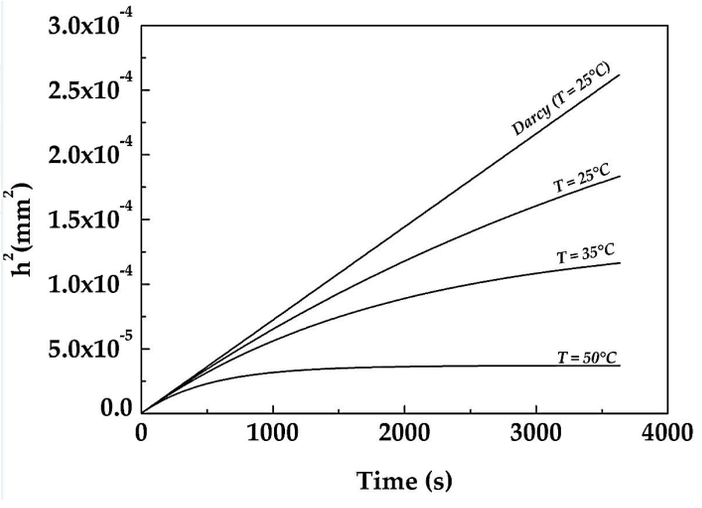

Figure 10. Evolution of the square of infiltration height with time for curing resins into porous preforms at different temperatures.

8. Concluding remarks

The present chapter has introduced the reader to the processes involved in the manufacture of different types of composite materials (PMCs, MMCs, CMCs) via infiltration. Over 90% of the world production of composite materials is carried out by infiltration, especially in the case of PMCs where it is almost the only available processing technique, while in case of metal matrix, production via infiltration represents only 70% [7]. In order to accurately control the properties of the final material and to be able to optimize the production, it is key to identify and understand the different processes involved in the manufacture of these materials. For this purpose, in this chapter, different models have been elucidated, starting from the differential equation of Navier-Stokes and taking into account the basic laws of wetting, by applying different real conditions often found in industry. For PMCs, the main discussed issue was the change in viscosity that thermoset matrixes experiment during infiltration. By introducing this phenomenon in the infiltration equations, it becomes clear that it can be a limiting factor during production since it shows a great deviation from Darcy's law. In the case of MMCs, the main phenomenon analyzed was the effect of saturation on infiltration. It became clear that variable saturation not only affects in a huge manner infiltration kinetics, but also changes the dominating phenomena. The last publications in this area have identified percolation as probably the leading phenomenon on infiltration in unsaturated systems at very low overpressure. Finally, for CMCs, the role of pore narrowing, an issue that has been widely discussed in the literature over the past 10 years was revised. This phenomenon is especially relevant in processing of ceramics and ceramic matrix composites via reactive techniques like the RBSC method used for SiC production. Even though the research on this area is vast, there is still not a full understanding of the effect of pore reduction on infiltration. Most models proposed still yield higher infiltration rates than the ones observed experimentally, because they do not consider the effect of chemical reactivity.

Appendix

Table 1 shows the main characteristic of the carbon particles used in this work.

Particle	D(90)	D(50)	D(10)	D(4,3)	D(3,2)	Span	V_p
P1	25.8	13.4	7.0	15.1	11.6	1.39	0.511
P2	41.0	25.8	15.5	27.2	23.0	0.99	0.515
P3	95.1	62.0	36.8	64.0	53.0	0.94	0.518
P4	173.6	117.6	56.6	124.1	110.4	0.99	0.482

Table 1. Main characteristics of the carbon particles used. Span is defined as D(90) − D(10)/D(50), where D(x) represents the diameter below which x% of particles are encountered. V_p is the particle volume fraction.

Table 2 shows the value of the parameters required to assess h(t) for the several cases exposed in this work. All parameters are in SI units.

http://dx.doi.org/10.5772/61167

Symbol	Magnitude	Value	SI units	Ref.
λ	Geometrical factor	2-4	-	[10, 21-23,25, 29]
a	Proportionality constant	$4 \cdot 10^{-4}$		[61]
γ_{lv}	Liquid-vapor surface tension of Si (at melting point)	0.750	N/m	[34-36]
θ	Contact angle of Si/C (at Si melting point)	40	°	[31]
η	Dynamic viscosity of molten Si (at melting point)	$0.605 \cdot 10^{-3}$	Pa·s	[34]
ϱ_{SIC}	Density of SiC	3210	kg/m^3	[9, 12]
M_{SiC}	Molar weight of SiC	$40 \cdot 10^{-3}$	kg/mol	[9, 12]
M_{Si}	Molar weight of Si	$28 \cdot 10^{-3}$	kg/mol	[9, 12]
$_{C/,SiC}$	Diffusion coefficient of C through SiC	$2 \cdot 10^{-14}$	m^2/s	[62]
ϱ_{SI}	Density of Silicon (at melting point)	2570	kg/m^3	[65]
k_s	kinetic constant in the SiC formation reaction	$4 \cdot 10^{-8}$	m/s	[71, 72]

Table 2. Value of the main parameters used in this work in SI units.

Acknowledgements

The authors would like to thank the University of Alicante for Danilo Sergi's scholarship under the program "Support for short stays of foreign researchers at the University of Alicante".

Financial support from the Generalitat Valenciana (PROMETEO II/2014/004- FEDER, Master grant "Santiago Grisolia" and PhD grant Vali+d), and the European Union's Seventh Framework Programme (FP7/2007-2013) under the HELM project (grant agreement no. 280464) is gratefully acknowledged.

Author details

Mario Caccia[1], Antonio Camarano[1], Danilo Sergi[2], Alberto Ortona[2] and Javier Narciso[1]

*Address all correspondence to: narciso@ua.es

1 University of Alicante, Department of Inorganic Chemistry, Apdo. Alicante, Spain

2 University of Applied Sciences SUPSI, The iCIMSI Research Institute, Manno, Switzerland

References

[1] Hull D, Clyne TW. An introduction to Composites Materials (2nd edn.). In: Clarke DR, Suresh S, Ward IM, (eds.), *Cambridge Solid State Series*. Cambridge: Cambridge University Press, 1996. p. 1 – 36. ISBN: 0 521 38190 8.

[2] Chung D. Composite Materials - science and applications (2nd edn.). In: Derby B (ed.), *Engineering Materials and Processes*. New York: Springer, 2010. p. 1 – 34. ISBN: 978-1-84882-830-8.

[3] Callister W Jr. Materials science and engineering: an introduction (6th edn.). In: Anderson W, Santor K, (eds.). *Wiley General Materials Science*. New York: Wiley & Son, 2000. p. 577 – 619. ISBN: 0-471-22471-5

[4] Chawla N, Chawla K. *Metal Matrix Composites*. In: Springer (ed.). Springer Science +Business Media New York: Springer-Verlag, 2006. p. 1 – 63. ISBN: 10 0-387-23306-7.

[5] Mallick P, Newman S. *Composites Materials Technology. Process and Properties*. In: Mallick P, Newman S (eds.). Hansel Publisher. Munich: Carl Hanser Verlag, 1990. p. 1 – 9. ISBN: 3-446-15684-4.

[6] Miracle D, Donaldson S. *ASM HandBook Volume 21 – Composites*. In: Moosbrugger Ch, Kinson J (eds.). ASM International. Materials Park (Ohio): ASM International Committee, 2001. p. 39 – 483. ISBN: 0-87170-703-9.

[7] Evans A, Marchi CS, Mortensen A. *Metal Matrix Composites in Industry: An Introduction and a Survey*. In: Springer group (ed.). Springer Science+Business Media. Dordrecht (Netherland): Kluwer Academic Publisher, 2003. p. 1 - 79 ISBN: 978-1-4020-7521-6

[8] Chawla K. *Composite Materials: Science and Engineering (Materials Research and Engineering)*. In: Springer (ed.). Materials Research and Engineering. New York: Springer, 2013. p. 1 – 176. ISBN-10: 0387743642.

[9] Narciso-Romero FJ, Rodríguez-Reinoso F, Díez MA. Influence of the carbon material on the synthesis of silicon carbide. *Carbon* 1999; 37(1):1771-1778. DOI: 10.1016/S0008-6223(99)00045-7

[10] Rodríguez-Guerrero A, Sánchez SA, Narciso J, Louis E, Rodríguez-Reinoso F. Pressure infiltration of Al–12wt.% Si–X (X= Cu, Ti, Mg) alloys into graphite particle preforms. *Acta Mater* 2006; 54(7):1821-1831. DOI: 10.1016/j.actamat.2005.11.041

[11] Narciso J, Alonso A, Pamies A, Garcia-Cordovilla C, Louis E. Factors affecting pressure infiltration of packed SiC particulates by liquid aluminum. *Metall Mater Trans A* 1995; 26(4): 983-990. DOI: 10.1007/BF02649095

[12] Calderon NR, Martinez-Escandell M, Narciso J, Rodríguez-Reinoso F. The role of carbon biotemplate density in mechanical properties of biomorphic SiC. *J Eur Ceram Soc* 2009; 29(3): 465-472. DOI: 10.1016/j.jeurceramsoc.2008.05.049

[13] Ortona A, Donato A, Filacchioni G, De Angelis U, La Barbera A, Nannetti CA, Riccardi B, Yeatman J. SiC–SiC f CMC manufacturing by hybrid CVI–PIP techniques: process optimization. *Fusion Eng Des* 2000; 51: 159-163. DOI:10.1016/S0920-3796(00)00310-0

[14] Nannetti CA, Ortona A, Pinto DA, Riccardi B. Manufacturing SiC-fiber-reinforced SiC matrix composites by improved CVI/slurry infiltration/polymer impregnation and pyrolysis. *J Am Ceram Soc* 2004; 87(7): 1205-1209. DOI: 10.1111/j.1551-2916.2004.tb20093.x

[15] Ortona A. Ceramic matrix composites: reaction bonded. In: Wiley (ed.). *Wiley Encyclopedia of Composites*. Manno (Switzerland): Wiley, 2011. p. 1 – 4. DOI: 10.1002/9781118097298.weoc031

[16] Kaczmara J, Pietrzakb K, Wlosinski W. The production and application of metal matrix composite materials. *J Mater Process Tech* 2000; 106: 58-67. doi:10.1016/S0924-0136(00)00639-7

[17] Harrigan Jr W. Commercial processing of metal matrix composites. *Mat Sci Eng A-Struct* 1998; 244: 75-79. DOI: 10.1016/S0921-5093(97)00828-9

[18] Miracle D. Metal matrix composites – from science to technological significance. *Compos Sci Technol* 2005; 65: 2526-2540. doi:10.1016/j.compscitech.2005.05.027

[19] Brooks RH, Corey AT. *Hydraulic Properties of Porous Media*. Hydrology papers Colorado State University. Fort Collins: Colorado State University; 1964; 5: 1-27.

[20] Van Genuchten M. A closed-form equation for predicting the hydraulic conductivity of unsaturated soils. *Soil Sci Soc Am J* 1980; 44(5): 892-898. doi:10.2136/sssaj1980.03615995004400050002x

[21] Garcia-Cordovilla C, Louis E, Narciso J. Pressure infiltration of packed ceramic particulates by liquid metals. *Acta Mater* 1999; 47(18): 4461-4479. DOI: 10.1016/S1359-6454(99)00318-3

[22] Alonso A, Pamies A, Narciso J, Garcia-Cordovilla C, Louis E. Evaluation of the wettability of liquid aluminum with ceramic particulates (SiC, TiC, AI2O3) by means of pressure infiltration. *Metall Trans A* 1993; 24 (6): 1423-1432. DOI: 10.1007/BF02668210

[23] Molina JM, Saravanan RA, Arpón R, Garcıa-Cordovilla C, Louis E, Narciso J. Pressure infiltration of liquid aluminium into packed SiC particulate with a bimodal size distribution. *Acta Mater* 2002; 50(2): 247-257. DOI: 10.1016/S1359-6454(01)00348-2

[24] Prieto R, Molina JM, Narciso J, Louis E. Fabrication and properties of graphite flakes/metal composites for thermal management applications. *Scripta Mater* 2008; 59(1): 11-14. DOI: 10.1016/j.scriptamat.2008.02.026

[25] Molina JM, Piñero E, Narciso J, García-Cordovilla C, Louis E. Liquid metal infiltration into ceramic particle preforms with bimodal size distributions. *Curr Opin Solid St M* 2005; 9(4): 202-210. DOI: 10.1016/j.cossms.2006.02.005

[26] Narciso J, Alonso A, Pamies A, Garcia-Cordovilla C, Louis E. Wettability of binary and ternary alloys of the system Al-Si-Mg with SiC particulates. *Scripta Metall Mater* 1994; 31(11): 1495-1500. DOI: 10.1016/0956-716X(94)90063-9

[27] Tian J, Piñero E, Narciso J, Louis E. Effects of temperature on pressure infiltration of liquid Al and Al–12wt.% Si alloy into packed SiC particles. *Scripta Mater* 2005; 53(12): 1483-1488. DOI: 10.1016/j.scriptamat.2005.07.038

[28] Molina JM, Arpón R, Saravanan RA, Garcıa-Cordovilla C, Louis E, Narciso J. Threshold pressure for infiltration and particle specific surface area of particle compacts with bimodal size distributions. *Scripta Mater* 2004; 51(6): 623-627. DOI: 10.1016/j.scriptamat.2004.05.009

[29] Piñero E, Molina JM, Narciso J, García-Cordovilla C, Louis E. The intrinsic permeability of packed SiC particles with monomodal and bimodal size distributions. *J Compos Mater* 2008; 42: 2795-2804. DOI:10.1177/0021998308096502

[30] Sánchez AS, Narciso J, Rodríguez-Reinoso F, Bernard D, Watson IG, Lee PD, Dashwood RJ. Characterization of lightweight graphite based composites using X-ray microtomography. *Adv Eng Mater* 2006; 8(6): 491-495. DOI: 10.1002/adem.200600101

[31] Eustathopoulos N, Nicholas MG, Drevet B. Wettability at High Temperatures. In: Cahn RW (ed.). *Pergamon Materials Series*. Cambridge: Pergamon; 1999. ISBN: 978-0-08-042146-9

[32] Saravanan RA, Molina JM, Narciso J, García-Cordovilla C, Louis E. Effects of nitrogen on the surface tension of pure aluminium at high temperatures. *Scripta Mater* 2001: 44 (6): 965–970. DOI: 1016/S1359-6462(00)00688-6

[33] Pamies A, Garcia-Cordovilla C, Louis E. The measurement of surface tension of liquid aluminium by means of the maximum bubble pressure method: the effect of surface oxidation. *Scripta Metall* 1984; 18 (9): 869-872. DOI: 10.1016/0036-9748(84)90251-5

[34] Amore S, Giuranno D, Novakovic R, Ricci E, Nowak R, Sobczak N. Thermodynamic and surface properties of liquid Ge–Si alloys. *Calphad*. 2014; 44: 95-101. DOI:10.1016/j.calphad.2013.07.014

[35] Novakovic R, Ricci E, Gnecco F, Giuranno D, Borzone G. Surface and transport properties of Au–Sn liquid alloys. *Surf Sci* 2005; 599: 230-247. DOI:10.1016/j.susc.2005.10.009.

[36] Egry I, Ricci E, Novakovic R, Ozawa S. Surface tension of liquid metals and alloys — recent developments. *Adv Colloid Interface Sci* 2010;159: 198-212. DOI:10.1016/j.cis.2010.06.009

[37] Bahraini M, Molina JM, Kida M, Weber L, Narciso J, Mortensen A. Measuring and tailoring capillary forces during liquid metal infiltration. *Curr Opin Solid St M* 2005; 9(4): 196-201. DOI: 10.1016/j.cossms.2006.02.007

[38] M Bahraini M, Weber L, Narciso J, Mortensen A. Wetting in infiltration of alumina particle preforms with molten copper. *J Mater Sci* 2005; 40(9-10): 2487-2491. DOI: 10.1007/s10853-005-1980-1

[39] Molina M, Rodriguez-Guerrero A, Bahraini M, Weber L, Narciso J, Rodriguez-Reinoso F, Louis E, Mortensen A. Infiltration of graphite preforms with Al–Si eutectic alloy and mercury. *Scripta Mater* 2007; 56(11): 991-994. DOI: 10.1016/j.scriptamat.2007.01.042

[40] Mortensen A, Masur LJ, Cornie JA, Flemings MC. Infiltration of fibrous preforms by pure metal. 1. Theory. *Metall Mater Trans A* 1989; 20(11): 2535-2547. DOI: 10.1007/BF02666688

[41] Masur LJ, Mortensen A, Cornie JA, Flemings MC. Infiltration of fibrous preforms by pure metal. 2. Experiment. M*etall Mater Trans A* 1989; 20(11): 2549-2557. DOI: 10.1007/BF02666689

[42] Michaud V, Mortensen A. Infiltration processing of fibre reinforced composites: governing phenomena. *Compos Part A-Appl S* 2001; 32(8): 981-996. DOI: 10.1016/S1359-835X(01)00015-X

[43] Richards LA. Capillary conduction of liquids through porous mediums. *Physics 1*. 1931; 1: 318-333. DOI: 10.1007/s10853-005-1950-7

[44] Benavente D. Locks P, García-del-Cura MA, Ordoñez S. Predicting the capillary imbibition of porous rocks from microstructure. *Transp Porous Med* 2002; 49: 59–76. DOI: 10.1023/A:1016047122877

[45] Szymkiewicz A. Modelling water flow in unsaturated porous media. In: Rowínski P (ed.), *GeoPlanet: Earth and Planetary Sciences*. Berlin: Springer: 2013. p. 9 -170 DOI: 10.1007/978-3-642-23559-7_2

[46] Bear, Jacob, Cheng, Alexander HD. Modeling Groundwater Flow and Contaminant Transport. In: Bear J, editor. Theory and Applications of Transport in Porous Media. New York: Springer: 2010. p. 109-247. DOI: 10.1007/978-1-4020-6682-5

[47] Bear J, Bachmat Y. Introduction to modeling of transport phenomena in porous media. In: Bear J (ed.), *Theory and Applications of Transport in Porous Media*. London: Kluwer Academic Publishers: 1990. p. 263 - 285. DOl: 10.1007/978-94-009-1926-6

[48] Bear J. Dynamics of fluids in porous media. In: Bear J (ed.) *Dovers Books on Physics and Chemistry*. New York: Dovers Publications: 1972. p. 119 – 186. ISBN:0-486-65675-6

[49] Louis E, Miralles JA, Molina JM. High temperature infiltration at low overpressures: Darcy's law, the slug-flow hypothesis and percolation. *J Mater Sci* 2015; 50: 1655-1665. DOI: 10.1007/s10853-014-8726-x

[50] Léger A, Molina-Jorda JM, Weber L, Mortensen A. Percolation and universal scaling in composite infiltration processing. *Mater Res Lett* 2015; 3(1): 7-15. DOI: 10.1080/21663831.2014.948692

[51] Dopler T, Modaressi A, Michauds V. Simulation of metal-matrix composite isothermal infiltration processing. *Metall Mater Trans B* 2000; 31(2): 225-234. DOI: 10.1007/s11663-000-0041-z

[52] Molina JM, Narciso J, Louis E. On the triple line in infiltration of liquid metals into porous preforms. *Scripta Mater* 2010; 62(12): 961-965. DOI: 10.1016/j.scriptamat.2010.03.015

[53] Rodríguez-Guerrero A, Molina JM, Rodríıguez-Reinoso F, Narciso J, Louis E. Pore filling in graphite particle compacts infiltrated with Al–12 wt.%Si and Al–12 wt.%Si–1 wt.%Cu alloys. *Mat Sci Eng A* 2008; 495: 276-281. DOI: doi:10.1016/j.msea.2008.01.071

[54] Michauds V. Mortensen A. On measuring wettability in infiltration processing. *Scripta Mater* 2007; 56(10); 859-862. doi:10.1016/j.scriptamat.2007.02.002

[55] Levenspiel O. Ingeniería de las Reacciones (2nd edn). Wiley (ed.). Barcelona: Revertre; 1978. ISBN: 84-291-7325-0

[56] Levenspiel O. El Omnilibro de los Reactores Químicos. Wiley (ed.). Barcelona: Revertre; 1986. ISBN: 84-291-7336-6

[57] Calderon NR, Martínez-Escandell M, Narciso J, Rodríguez-Reinoso F. The combined effect of porosity and reactivity of the carbon preforms on the properties of SiC produced by reactive infiltration with liquid Si. *Carbon* 2009; 47(9): 2200-2210. DOI: 10.1016/j.carbon.2009.04.002

[58] Voytovych R, Bougiouri V, Calderon NR, Narciso J, Eustathopoulos N. Reactive infiltration of porous graphite by NiSi alloys. *Acta Mater* 2008; 56(10): 2237-2246. DOI: 10.1016/j.actamat.2008.01.011

[59] Calderon NR, Voytovych R, Narciso J, Eustathopoulos N. Wetting dynamics versus interfacial reactivity of AlSi alloys on carbon. *J Mater Sci* 2010; 45(8): 2150-2156. DOI: 10.1007/s10853-009-3909-6

[60] Bougiouri V, Voytovych R, Rojo-Calderon N, Narciso J, Eustathopoulos N. The role of the chemical reaction in the infiltration of porous carbon by NiSi alloys. *Scripta Mater* 2006; 54(11): 1875-1878. DOI: 10.1016/j.scriptamat.2006.02.015

[61] Calderon NR, Voytovych R, Narciso J, Eustathopoulos N. Pressureless infiltration versus wetting in AlSi/graphite system. *J Mater Sci* 2010; 45(16): 4345-4350. DOI: 10.1007/s10853-010-4358-y

[62] Mortensen A, Drevet B, Eustathopoulos N. Kinetics of diffusion-limited spreading of sessile drops in reactive wetting. *Scripta Mater* 1997; 36(6): 654-651.

[63] Landry K, Eustathopoulos N. Dynamics of wetting in reactive metal/ceramic systems: linear spreading. *Acta Mater* 1996; 44(10): 3923-3932. DOI: 10.1016/S1359-6454(96)00052-3

[64] Dezellus O, Hodaj F, Eustathopoulos N. Chemical reaction-limited spreading: the triple line velocity versus contact angle relation. *Acta Mater* 2002; 50(19): 4741-4753. DOI: 10.1016/S1359-6454(02)00309-9

[65] Dezellus O, Jacques S, Hodaj F, Eustathopoulos N. Wetting and infiltration of carbon by liquid silicon. *J Mater Sci* 2005; 40(10): 2307-2311. DOI: 10.1007/s10853-005-1950-7

[66] Bougiouri V, Voytovych R, Dezellus O, Eustathopoulos N. Wetting and reactivity in Ni-Si/C system: experiments versus model predictions. *J Mater Sci* 2007; 42(6): 2016-2023. DOI: 10.1007/s10853-006-1483-8

[67] Sergi D, Grossi L, Leidi T, Ortona A. Surface growth effects on reactive capillary-driven flow: Lattice Boltzman investigation. *Eng Appl Comp Fluid* 2014; 8(4): 549-561. DOI: 10.1080/19942060.2014.11083306

[68] Sergi D, Grossi L, Leidi T, Ortona A. Lattice Boltzmann simulations on the role of channel structure for reactive capillary infiltration. *Cond Mat Soft* 2014: arXiv: 1409.0954

[69] Bowman JM, Buffenbarger R, Clark J, Embrekts L, Goldberg S, Lambert S. Advanced materials by design. In: Nichols RW (ed.). *U.S. Congress, Office of Technology Assessment*. Washington, DC: U.S. Government Printing Office, 1988. NTIS order #PB88-243548

[70] Cañamero-Martínez P, Fernández-García M, Fuente JL. Rheological cure characterization of a polyfunctional epoxy acrylic resin. *React Funct Polym* 2010; 70: 761-766. doi:10.1016/j.reactfunctpolym.2010.07.010

[71] Fitzer E, Gadow R. Investigations of the reactivity of different carbons with liquid silicon. In: *Proceedings of International Symposium on Ceramic Components for Engines; 1983, Japan*. Tokyo, Japan: KTK Scientific publishers; 1984. p. 561-572.

[72] Messner RP, Chiang Y. Liquid-phase reaction-bonding of silicon carbide using alloyed silicon-molybdenum melts. J Am Ceram Soc 1990; 73(151): 1193-1200. DOI: 10.1111/j.1151-2916.1990.tb05179.x

IntechOpen